Received: 12 March 2026 | Revised: 27 June 2026 | Accepted: 9 July 2026

DOI: 10.1002/rpm2.70074

RESEARCH ARTICLE

RESPONSIVE MATERIALS Open Access WILEY

Natural antibacterial silk produced by feeding silkworms with human hair derived carbon dots

Zhao-Fan Wu[1] | **Xiao-Feng Shi**[2] | **Xiao-Xiao Luo**[1] | **Xi-Rong Zhang**[1] | **Yuan-Qing Mao**[2] | **Huan-Ming Xiong**[1]

[1]Department of Chemistry, Shanghai Key Laboratory of Electrochemical and Thermochemical Conversion for Resources Recycling, Fudan University, Shanghai, China

[2]Department of Orthopedics, Shanghai Ninth People's Hospital, Shanghai Key Laboratory of Orthopaedic Implants, Shanghai Jiao Tong University School of Medicine, Shanghai, China

Correspondence

Yuan-Qing Mao and Huan-Ming Xiong.
Email: MAOYQ1975@sh9hospital.org.cn and hmxiong@fudan.edu.cn

Abstract

Mulberry silk has exceptional mechanical properties and biocompatible nature, but suffers from its poor antibacterial capacity as protein fiber, a nutrient-rich environment for bacterial growth. Endowing the natural silk with antibacterial properties while preserving its inherent advantages remains a longstanding challenge. In this study, blue fluorescence carbon dots (B-CDs) are prepared from *Crinis carbonisatus*, which is derived from calcination of human hair and has been used as the traditional Chinese medicine for about 1800 years. Such B-CDs exhibit robust *Staphylococcus aureus*-inhibiting activity, and thus they are employed as feed additives for silkworms. The experimental silkworms show blue fluorescence in their bodies, cocoons, and even as moths, while the dissection of silkworms confirms the transport of B-CDs from the digestive tract to the silk gland. The degummed silk possesses visible blue fluorescence and anti-*S. aureus* properties, while retaining its inherent mechanical properties. Notably, B-CDs also regulate the secondary structure of silk proteins and upregulate the antibacterial protein contents, resulting in a synergistic antibacterial effect. As a result, the B-CDs@silk can accelerate wound healing, which outperforms the conventional gauze. In addition, B-CDs show no observable adverse effects on silkworm or rat health, indicating their biocompatibility and biosafety preliminarily.

Keywords

antibacterial silk, carbon dots, fluorescence, silkworm, wound healing

1 | INTRODUCTION

Mulberry silk, renowned as the "Queen of Fibers," has been widely used in the global textile industry for centuries owing to its exceptional mechanical properties, unique luster, and scalable production.[1,2] In the past decades, the applications of silk have been expanded to the electronics and optics fields,[3,4] especially the biomedical field due to its inherent biocompatibility and degradability. To date, various silk-based biomaterials have been developed, including fibroin nanospheres, tissue engineering scaffolds, medical sutures/gauze, and biological adhesives.[5–7] However, sericin readily absorbs water and provides nutrients for bacteria, and the residual fibroin after degumming remains susceptible to bacterial colonization due to its hydrophilic groups and porous structure,[8–10] hindering its applications in medical and hygienic products.[11,12] *Staphylococcus aureus* is a conditional pathogen widespread in nature and commonly found on human skin, whose infections can cause persistent wound complications and are increasingly associated with

Zhao-Fan Wu and Xiao-Feng Shi contributed equally to the work.

antibiotic resistance.[13–15] Therefore, endowing the natural silk with efficient, stable, biosafe, and antibacterial properties holds significant importance to expand its practical utility.

To date, post-treatment modification via physical adsorption or chemical functionalization remains the predominant approach, yet these methods may compromise the secondary structure and mechanical properties of silk, and are further hampered by uneven grafting and unstable performance.[16–19] Therefore, imparting antibacterial activity during silk formation in silkworm body offers a desirable route to preserve its intrinsic properties, and feeding silkworms with functional additives is generally considered more practical, efficient, and cost-effective compared with genome modification, while avoiding genetic pollution.[20–22] In the past decade, the functionalized silk with enhanced fluorescence, electrical conductivity, mechanical or thermal properties has been realized by this strategy.[22–27] However, these previous reports share common limitations: low intake-to-silk conversion rates, loss of additives during degumming, and particular difficulty in finding antibacterial additives that are nontoxic to silkworms and environmentally benign.[28] Therefore, it remains challenging to identify additives that are nontoxic to silkworms, compatible with fibroin, capable of improving silk antibacterial properties, and exhibiting high intake-to-silk conversion rates.

Carbon dots (CDs) are a class of fluorescent nanoparticles with carbon cores and various surface groups,[29] prepared by either top-down or bottom-up methods,[30] and have been explored as silkworm feeding additives owing to their biosafety and biocompatibility.[31,32] Antibacterial CDs are usually prepared by adsorbing metal ions or antibiotics, synthesized from some organic molecules, or extracted from Chinese herbal medicines in which the CDs are produced by the heat treatment on biomass.[33–35] The first two approaches are unsuitable for silkworm feeding, because the excretion of metal ions or antibiotics from silkworm bodies will pollute the environment, and many synthetic products are toxic to silkworms. In contrast, CDs derived from herbal medicines exhibit good biocompatibility and environmental friendliness, which have been applied widely in bioimaging, drug delivery, and phototherapy.[36] Liu et al. and John et al. synthesized CDs from mulberry leaves individually, and obtained functionalized silk via silkworm feeding. The former produced visibly red fluorescent silk using CDs with a quantum yield of 73%,[22] while the latter achieved dopamine-sensing silk via CDs with a ratiometric fluorescence response.[37] However, imparting antibacterial activity to silk by feeding silkworms with biomass-derived CDs remains unexplored. *C. carbonisatus*, a traditional Chinese medicine prepared by calcining human hair, has been used to treat hemorrhagic disorders for centuries and has been reported to possess hemostatic, antibacterial, and anti-inflammatory properties,[38–40] which make them a good candidate for synthesizing antibacterial CDs.

In this study, blue-emitting carbon dots (B-CDs) obtained by reflux extraction from calcined human hair (*C. carbonisatus*) are employed as silkworm feeding additives to produce intrinsically anti-*S. aureus* silk, as illustrated in Scheme 1. The degummed modified silk was able to promote tissue repair and regeneration in *S. aureus*-infected rat skin wound, outperforming conventional medical gauze. Compared with previous studies on biomass-derived CDs fed to silkworms, a notable contribution of the present work is the introduction of anti-*S. aureus* activity into silk via CDs, achieved through a cooperative mechanism involving both B-CDs and upregulated antibacterial proteins in silk. Within the scope of the current evaluation, B-CDs did not exhibit significant adverse effects on the growth, development, and reproduction of silkworms, nor on rat health during wound healing, and the entire process is basically safe and environmentally friendly. More importantly, the intake-to-silk conversion rate of B-CDs reaches 32% and the B-CDs content in the degummed silk is up to 1.5 wt.%, indicating an efficient translocation of additives from ingestion to silk fiber within the silkworm body.

2 | RESULTS AND DISCUSSION

2.1 | Characterizations of B-CDs

B-CDs are black powder that can be dispersed in ethanol easily, and the obtained clear solutions are used for the subsequent measurements. Transmission electron microscopy (TEM) images reveal that B-CDs are uniform monodispersed spherical nanoparticles (Figure 1a), while the inset high-resolution TEM image and Figure S1 show the clear lattice fringes with an interplanar spacing of 0.21 nm, corresponding to the (100) crystal plane of graphitic carbon.[41] The statistical analysis indicates that most of B-CDs' diameters distribute in the range of 3.8 ± 0.4 nm (Figure 1b). The color of the ethanol solution deepens gradually as the B-CDs concentration increases, but all the solutions show bright blue fluorescence under ultraviolet (UV) light (Figure S2). When the excitation wavelength changes from 300 to 400 nm, the emission peak of B-CDs remains in the blue light region (410–480 nm), and the optimal excitation/emission wavelengths are determined to be 365/420 nm. The UV-vis absorption spectrum in Figure 1c shows that, B-CDs have strong absorption in the UV light region with a sharp peak at 220 nm, corresponding to the π-π* transition of C=C bonds within the CDs,[42] which is widely regarded as the fluorescence origin of the typical CDs. The oil-water partition coefficient (Log *D*) of B-CDs is determined via the shake-flask method (detailed procedures are provided in the Supporting Information S1).[43] Figure 1d shows the standard curves of B-CDs in phosphate buffered saline and *n*-octanol respectively, with black points used and red points excluded. The optimal absorbance exhibits a linear relationship with the concentration, and the linear increase rate is steeper in *n*-octanol, indicating the greater solubility of B-CDs in *n*-octanol. The preferential partition of B-CDs into the *n*-octanol phase is also directly visualized under UV light

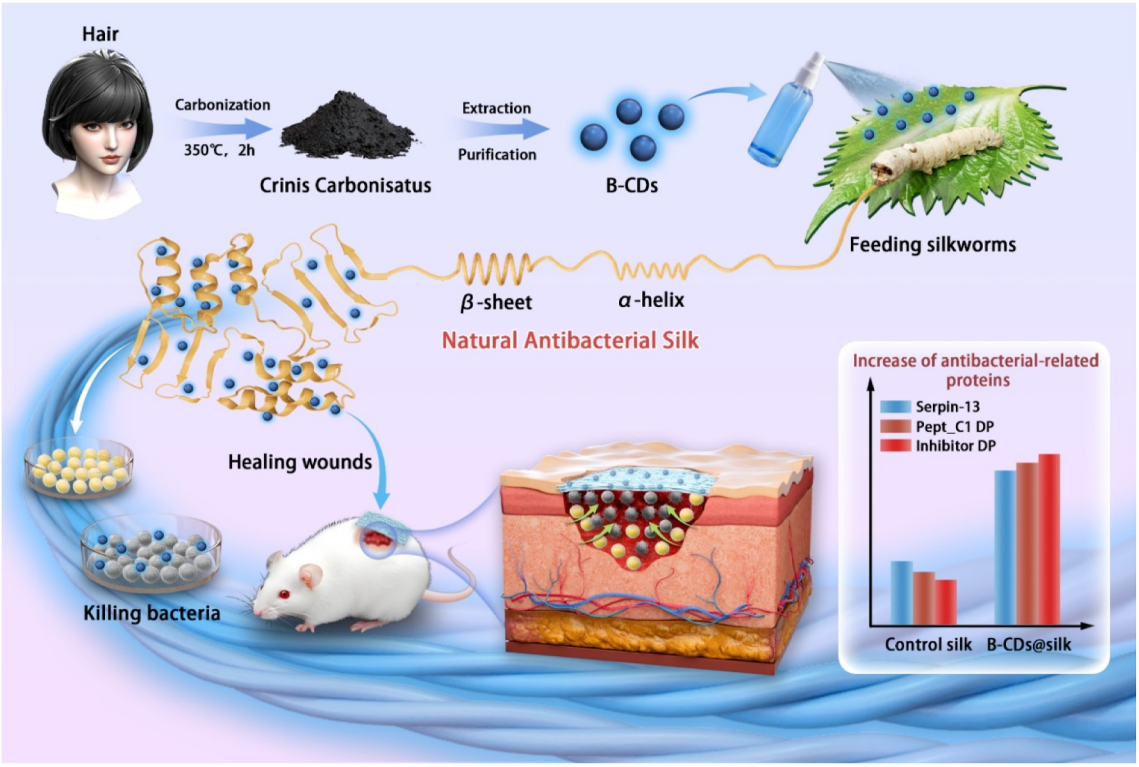

SCHEME 1 Human hair derived B-CDs are sprayed onto mulberry leaves for feeding silkworms to produce B-CDs@silk, which are used for killing *Staphylococcus aureus* and healing wounds on animal skin. The medical performance of B-CDs@silk results from the antibacterial properties of B-CDs and the increase of antibacterial proteins in natural silk. B-CDs, blue fluorescence carbon dots.

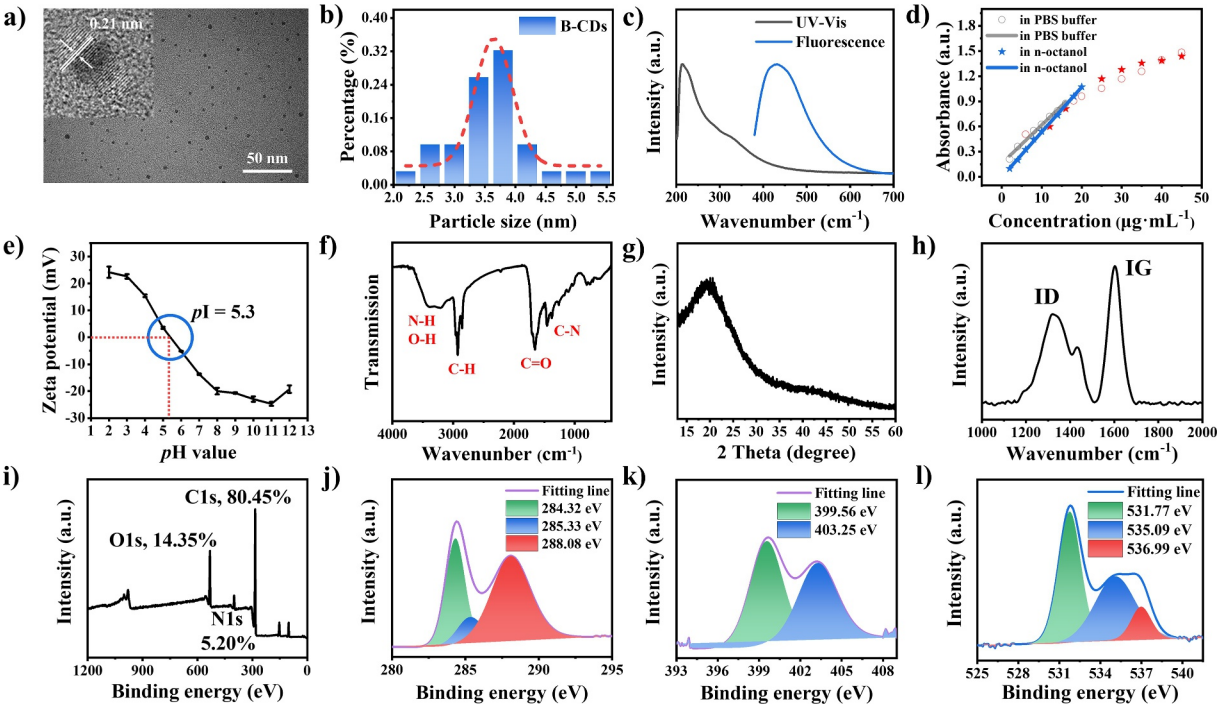

FIGURE 1 Characterization results of B-CDs. (a) TEM and high-resolution TEM (inset) images, (b) particle size distribution, (c) UV-vis and fluorescence spectra of B-CDs, respectively. (d) Standard curves of B-CDs in PBS buffer (Abs = 0.0459 × c + 0.1571, Abs = 0.1711, c = 0.3044 μg·mL^{-1}) and n-octanol (Abs = 0.0536 × c − 0.0019, Abs = 0.1611, c = 3.0416 μg·mL^{-1}). (e) Zeta potential of B-CDs in aqueous solutions with different pH values. (f) FTIR spectrum of B-CDs. (g) X-ray diffraction patterns, (h) Raman spectra, (i) XPS full spectra of B-CDs, respectively. Deconvolution results for the high-resolution XPS of (j) C 1s, (k) N 1s, and (l) O 1s of B-CDs, respectively. B-CDs, blue fluorescence carbon dots; FTIR, fourier transform infrared; PBS, phosphate buffered saline; TEM, transmission electron microscopy; UV, ultraviolet; XPS, X-ray photoelectron spectroscopy.

(Figure S3). Calculations on the standard curves present a Log *D* value of about 1, indicating strong lipophilicity that is required for feeding silkworms. The zeta potential of B-CDs shifts from positive to negative as the pH value of the solution increases, and thus the isoelectric point is determined to be 5.3 (Figure 1e), which means B-CDs have weak acidic surface groups that facilitate B-CDs enrichment in silk glands.[44] Furthermore, the fluorescence of B-CDs remains relatively stable across a pH range from 2 to 13, with maximum intensity near the isoelectric point (pH 5, Figures 1e and S4) and a negligible decline toward alkaline conditions, supporting their applicability in complex physiological environments. Fourier transform infrared (FTIR) spectra of B-CDs (Figure 1f) exhibit a broad peak at 3200–3600 cm^{-1}, two sharp peaks at 2927 and 2851 cm^{-1}, an intense peak at 1654 cm^{-1}, and a weak peak at 1455 cm^{-1}, that are assigned to O–H/N–H, alkyl C–H, C=O, and C–N stretching vibrations, respectively.[45,46]

X-ray diffraction patterns (Figure 1g) of B-CDs show a broad peak at around 22°, corresponding to the typical amorphous carbon structure of CDs.[47] Raman spectra of B-CDs (Figure 1h) reveal two peaks at 1318 cm^{-1} (D-band, disordered carbon) and 1592 cm^{-1} (G-band, graphitic carbon) respectively, with an additional small sharp peak adjacent to the D-band, which are also characters of CDs.[48] It is clear that B-CDs have higher graphitization degrees than those CDs synthesized from organic substances hydrothermally. X-ray photoelectron spectroscopy (XPS) data demonstrate that B-CDs (Figure 1i) are mainly composed of C, N, and O elements, with atom ratios of 80.45%, 5.20%, and 14.35%, respectively. The C 1s spectra (Figure 1j) can be deconvoluted to C–C (284.32 eV), C–O–C (285.33 eV), and O–C=O (288.08 eV) bands. The N 1s spectra (Figure 1k) can be deconvoluted to C–N (399.72 eV) and N–O (403.23 eV) bands. The O 1s spectra (Figure 1l) can be deconvoluted to C=O (531.77 eV), C–O (535.09 eV), and O–H (536.99 eV) bands.[49,50] These high-resolution XPS analyses are consistent with the above FTIR results.

2.2 | Fluorescent silkworms and their silk

B-CDs represent a suitable choice for feeding silkworms to produce naturally modified silk, owing to their high yield, suitable lipophilicity and stable fluorescence. Silkworms were first reared normally on common mulberry leaves until the third day of the fifth instar. Subsequently, the silkworms were divided into one control group and four experimental groups that are designated as Control (without B-CDs), B-CDs0.05‰, B-CDs0.1‰, B-CDs0.2‰, and B-CDs0.5‰, respectively, according to the mass ratios of the B-CDs additive to the mulberry leaves. Figure S5 illustrates the complete silkworm life cycle, including the egg hatching, the development from the first to the fifth instar, the cocooning, the eclosion, the mating, and the oviposition. The blue fluorescence can be seen clearly during the silkworm spinning process (Figure 2a) and in the subsequent moth bodies (Figure 2b). In contrast, the control group shows no blue fluorescence for the cocooning silkworms and the adult moths (Figures S6 and S17). In addition, only feeding a tiny amount of B-CDs (0.5 wt.‰ in mulberry leaves) can obtain the cocoons with uniform blue fluorescence (Figure 2d). Fluorescence spectra of cocoons from the control, the low-intake (B-CDs0.1‰), and the high-intake (B-CDs0.5‰) groups (Figure 2c) show a gradual increase of blue fluorescence intensity at 420 nm under the same excitation wavelength. When these cocoons are shredded and soaked in dichloromethane (DCM) respectively, such difference becomes clear: the control is yellow–green and the experimental group shows bright blue fluorescence (Figures 2e and S7), consistent with their fluorescence spectra (Figure 2f), respectively.

The TEM images of the DCM extract from the experimental group (Figure 2g) show numerous uniform spherical nanoparticles with the lattice fringes of 0.21 nm, which prove B-CDs have been ingested by silkworms and transferred to cocoons finally. Since the silk used in practical applications is fibroin fiber, the B-CDs additives must retain in the degummed silk after the cocoon cooking process.[51] The fluorescence spectra of the degummed silk (Figure 2h) show that the intensity of blue fluorescence enhances as the B-CDs concentration increases. In Figures 2i, S7 and S8, the control cocoons exhibit light yellow/green fluorescence and their degummed silk looks dim purple under UV light, while in the experimental group both the cocoons and the degummed silk show bright blue fluorescence. Laser scanning confocal microscopy was used to observe the degummed silk in the dark field (laser: 405 nm; emission: 415–500 nm) and the bright field, respectively (Figure 2j). After filtering out the violet light, both the control and the B-CDs0.5‰ sample exhibit blue fluorescence, but the intensity of the latter is about 3 times of that of the control (Figure 2k). The above results confirm that B-CDs have been incorporated into fibroin fibers which keep stable fluorescence even after the degumming treatment (boiling in the alkaline aqueous solution for hours).

2.3 | Characterizations of B-CDs@silk

Scanning electron microscopy (SEM)[52] images (Figures 3a and S9) show that, the degummed silk from the control and the experimental group looks the same, and there are no particles or aggregates around, indicating the B-CDs have incorporated inside the silk. Statistical analyses on different groups of silk (Table S1) present an average diameter of ~9.5 μm (consistent with the data in literature)[23] for both the control and the experimental groups, suggesting that B-CDs incorporation has no influence on the diameter and surface morphology of the silk. Figures 3b and S10 present the stress–strain curves of the degummed silk from the five groups (20 silk fibers per group). Four mechanical parameters are statistically calculated from these curves and listed in Table S2. When the B-CDs content increases gradually from the control to the experimental groups, the tensile strength of

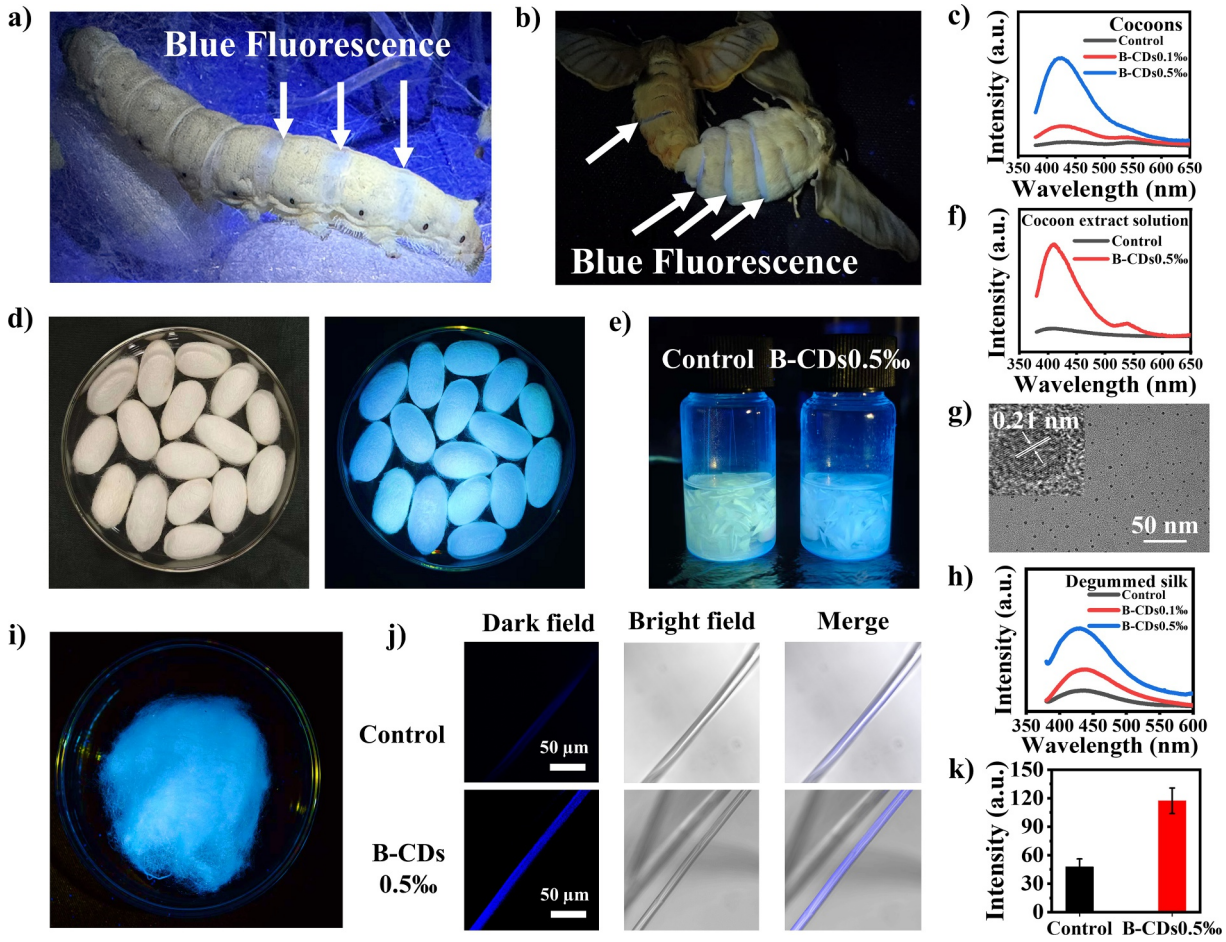

FIGURE 2 The internal B-CDs endow bright fluorescence to the silkworms, moths and silks. (a) The experimental silkworms are spinning cocoons, and (b) the silkworm moths are mating, under UV light respectively. (c) Fluorescence spectra of silkworm cocoons from the control group and two experimental groups, respectively. (d) B-CDs-modified cocoons under room light (left) and UV light (right), respectively. (e) DCM (CH_2Cl_2) extracts from cocoons of the control (left) and B-CDs0.5‰ group (right) under UV light, and (f) their fluorescence spectra. (g) TEM and high-resolution TEM images of DCM extracts from the B-CDs0.5‰ cocoons. (h) Fluorescence spectra of the degummed silk fibers from the control group and two experimental groups, respectively. (i) The degummed silk from B-CDs0.5‰ group under UV light. (j) Laser scanning confocal microscopic images of the degummed silk fibers from the control group and B-CDs0.5‰ group, respectively, and (k) their average fluorescence intensity. B-CDs, blue fluorescence carbon dots; DCM, dichloromethane; TEM, transmission electron microscopy; UV, ultraviolet.

silk decreases, the elongation at break of silk increases (Figure 3c), Young's modulus of silk decreases slightly overall (Figure S11a), and the fracture work of silk keeps consistent relatively (Figure S11b). These results confirm that B-CDs incorporation do not influence the intrinsic mechanical properties of natural silk significantly.

It is well known that silk fibroin is a semicrystalline material with three secondary structures: α-helix/amorphous, β-sheet, and β-turn. Among them, the dense β-sheets (crystalline phase) confer high tensile strength to silk, while the ordered distribution of β-sheets and amorphous regions (amorphous phase) contribute to its good elongation. These secondary structures of silk can be characterized by FTIR analyses.[2,24,25] Figure 3d,e show that both the cocoons and the degummed silk exhibit characteristic peaks of fibroin: 1697 (β-turn), 1616 and 1227 cm^{-1} (β-sheets), and 1265 cm^{-1} (random coil/α-helix).[53,54] The above evidence demonstrates that the introduction of B-CDs does not alter the scaffold structure of silk, and that B-CDs interact with the protein via non-covalent interactions (hydrogen bonds and intermolecular forces).[24] In Figure 3d, the 1616 cm^{-1} peak in amide I band becomes broader and shifts to the higher wavenumbers when the B-CDs content in silk increases. This trend is more pronounced in the magnified FTIR spectra, which exhibit broader peaks for cocoons (Figure 3d) and higher wavenumber shifts for the degummed silk (Figure 3e). FTIR deconvolution of the amide I band (Figures S12 and S13) reveal three sub-peaks: 1630 cm^{-1} (random coil/α-helix), 1660 cm^{-1} (β-sheet), and 1690 cm^{-1} (β-turn). The contents of each structure are calculated by quantifying the deconvoluted peak areas, respectively.[18,23] These content differences are most significantly manifested between the degummed silk in the control group and that in B-CDs0.5‰ group (Figure 3f). When more and more B-CDs are incorporated, the α-helix content increases while the β-sheet content decreases in both the raw silk (Figure S14) and

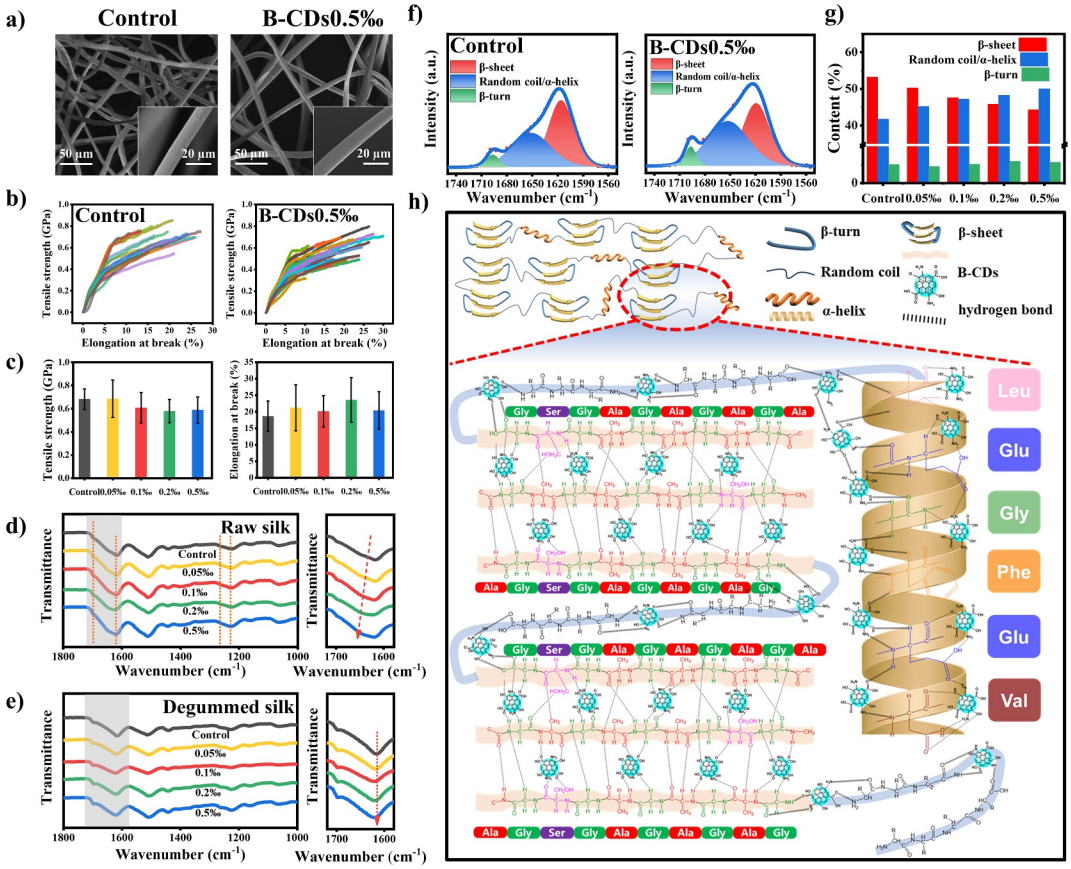

FIGURE 3 Morphologies, mechanical properties and internal structures of B-CDs@silk. (a) Scanning electron microscopy images of the degummed silk fibers in the control and B-CDs0.5‰ group, respectively (scale bar: 50 μm). The insets are single silk fibers with a scale bar of 20 μm. (b) Stress–strain curves measured from 20 degummed silk fibers, which were sampled as 6–7 fibers per cocoon with 3 cocoons included in the control and B-CDs0.5‰ group, respectively. (c) Statistical analysis of the tensile strength and the elongation at break of degummed silk fibers (tensile rate: 2 mm/min). (d) FTIR spectra (left) with the local spectra (right) of the raw silk (non-degummed) fibers. (e) FTIR spectra (left) with the local spectra (right) of the degummed silk fibers. (f) Deconvolution results of FTIR spectra in the amide I band of the degummed silk fibers in the control and B-CDs0.5‰ group, respectively. (g) Statistical analyses on the content of different protein secondary structures for the degummed silk fibers obtained by deconvolution calculation of the amide I-band. (h) Schematic diagram of the interaction mechanism between B-CDs and the three secondary structures of silk via non-covalent interactions (hydrogen bonding). B-CDs, blue fluorescence carbon dots; FTIR, fourier transform infrared.

the degummed silk (Figure 3g). This trend corresponds to the decrease in silk tensile strength and the increase in elongation at break simultaneously. It can be inferred that B-CDs incorporation inhibits the conversion of silk fibroin from a random coil/α-helix state to *β*-sheet crystals, thereby increasing the amorphous region, enhancing silk elongation, and providing more binding sites for B-CDs.[19,55,56] According to Figure 1f, it is observed that the surface of B-CDs contains amino, carboxyl, and hydroxyl groups, which can form hydrogen bonds with the amino acids composing the silk protein. Figure 3h illustrates the binding mechanism between B-CDs and silk proteins. It is known that, apart from the *β*-sheet with a regular amino acid sequence (Gly-Ser-Gly-Ala-Gly-Ala), other conformations lack specific sequences (represented by R).[57] The B-CDs embed between the folded layers of the *β*-sheet via hydrogen bonds (N···H, C=O···H, etc., depicted as dashed lines) and attach to the surface of the random coil/*α*-helix and *β*-turn peptide chains. Additionally, B-CDs may act as bridges between different conformations, facilitating conformational sliding and preventing the transformation of *α*-helix to *β*-sheet, which results in an increase in the amorphous region and an enhancement in the elongation at break.

2.4 | In vitro anti-*S. aureus* activity and in vivo wound healing effects of B-CDs@silk

To evaluate the antibacterial efficacy of the degummed silk, the sterilized samples were co-cultured with *S. aureus* for 4 h using the spread plate assay. In Figure 4a, compared with the blank control (no silk added), the bacteria co-cultured with the raw silk proliferate rapidly, which means the natural silk not only lacks antibacterial activity but also adsorbs bacteria, providing nutrients for bacterial reproduction and thus acting as a "hotbed" for the bacterial growth.[58,59] In contrast, the bacterial proliferation was significantly inhibited when the silk from the B-CDs0.1‰ group was tested. When the B-

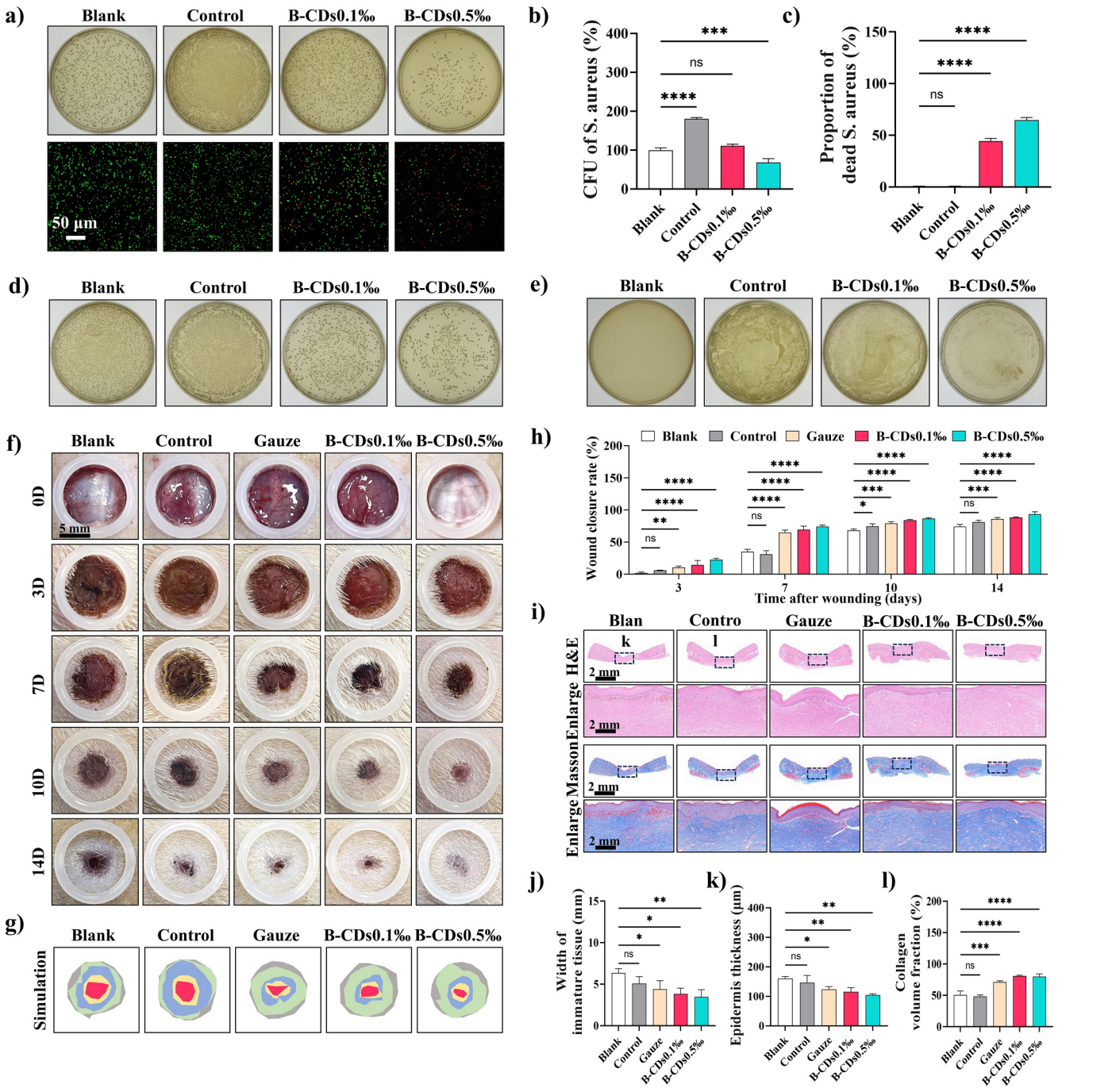

FIGURE 4 In vitro assessment of anti-*Staphylococcus aureus* activity and in vivo wound healing efficacy of the degummed silk in Sprague-Dawley (SD) rats. (a) Antibacterial efficacy of the degummed silk against *S. aureus* determined by colony forming unit (CFU) enumeration. Live/dead fluorescence staining of *S. aureus* incubated with the degummed cocoons. (b) Quantitative analysis of bacterial CFUs. Data are presented as mean ± SD ($n = 3$). Significance levels: $^{*}p < 0.05$, $^{**}p < 0.01$, $^{***}p < 0.001$, $^{****}p < 0.0001$. (c) Proportion of dead *S. aureus* cells ($n = 3$). (d) Antibacterial efficacy of the degummed silk after 3 months of storage against *S. aureus* determined by CFU enumeration. (e) Bacterial adhesion on the surface of silk from different groups in a natural humid environment. (f) Representative wound photographs at 0-, 3-, 7-, 10-, and 14-days post-surgery. (g) Wound healing schematic following different treatments. (h) Healing rate analyses ($n = 3$). (i) Hematoxylin and eosin and Masson's trichrome staining of the healed tissues. (j–l) Quantitative histomorphometric analyses on (j) granulation tissue width, (k) epidermal thickness, and (l) collagen volume fraction ($n = 3$), respectively.

CDs0.5‰ group was applied, bacteria were not only inhibited from proliferating but also killed in large numbers. The bottom pictures in Figure 4a are confocal fluorescence images of bacteria after the live/dead staining fluorescein isothiocyanate/propidium iodide. Figure 4b presents the statistical results in Figure 4a, while Figure 4c provides the dead bacteria ratio analysis. These results confirm the raw silk has no antibacterial effect, but the B-CDs@silk reduces live bacteria (green fluorescence) and increases dead bacteria (red fluorescence) simultaneously. Such an antibacterial performance

improves as the B-CDs content in the silkworm feeding increases. To test the antibacterial stability of these samples, the same tests were performed after storing the degummed silk for 3 months, and the results show their antimicrobial properties were sufficiently retained (Figure 4d). Figure 4e shows the naturally bacterial attachment on the silk surface after 3 days of exposure to a humid environment (the bacterial species are unidentified, and only colony count is discussed). It was observed that at 80% humidity, bacteria in the air adhered to the silk and proliferated extensively, whereas the bacterial growth on the B-CDs@silk surface was very slow. Furthermore, the more the incorporation of B-CDs, the better the antibacterial effect. This experiment confirms that B-CDs@silk is able to reduce the adhesion and proliferation of airborne bacteria on silk surfaces in daily life environments.

Clinically, naturally occurring *S. aureus* colonizing wound sites induces inflammatory reactions and biofilm formation, which impede tissue regeneration.[60,61] The B-CDs@silk developed in this study can inhibit bacterial proliferation and eliminate the pathogen, creating a favorable microenvironment for wound healing, accelerating neotissue regeneration.[62] To evaluate its application potential in medical antibacterial gauze/sutures, a full-thickness skin defect healing model was established on Sprague-Dawley rats. 10 mm-diameter circular full-thickness wounds were created on the skin of rats, which were divided into five groups (4 rats/group): Blank (no treatment), Control (covered with the degummed raw silk), Gauze (covered with conventional medical gauze), Low-concentration B-CDs (covered with the degummed silk from silkworms fed with B-CDs0.1‰), and High-concentration B-CDs (covered with the degummed silk from silkworms fed with B-CDs0.5‰). Over the 2-week observation period (Figure 4f), B-CDs-free silk showed marginal benefit over the Blank group by day 7 but remained less effective than medical gauze. By day 10, wound areas in the B-CDs0.1‰ and B-CDs0.5‰ groups were notably smaller than those in the Control and Gauze groups, and by day 14, wounds in the B-CDs0.5‰ group were nearly fully closed with fur restored, while residual wounds persisted in the other groups. The simulated wound images of each group at different days (Figure 4g), along with quantitative analyses on the recovery rate (Figure 4h), were consistent with the above observations. After 14 days, the peri-wound tissues were harvested from each group for the pathological assessment. H&E staining (Figure 4i) reveals that all wounds have progressed to the late proliferative phase, with B-CDs-modified groups showing more regularly organized granulation tissue aligned parallel to wound margins, no epidermal hyperproliferation, and restored epidermal thickness. Quantitative analyses (Figure 4j,k) further confirm superior wound recovery in the B-CDs0.5‰ group. Masson's trichrome staining (Figure 4i) shows the most abundant and dense collagen deposition in B-CDs@silk-treated wounds, indicating granulation tissue maturation, while Blank/Control/Gauze groups show uneven staining and intracollagen gaps, consistent with incomplete healing. The collagen volume fraction (Figure 4l) further confirms enhanced collagen deposition in the B-CDs@silk group. Our previous work has demonstrated that CDs derived from *C. carbonisatus* can regulate the wound microenvironment by inhibiting the release of inflammatory factors such as TNF-α and IL-1β and reduce reactive oxygen species levels, and influence the PI3K-Akt signaling pathway, thereby promoting neovascularization.[40]

2.5 | Antibacterial mechanism and proteomic analysis of B-CDs@silk

To investigate the antibacterial mechanism of B-CDs@silk against *S. aureus*, SEM was performed to examine bacterial morphology and adhesion density on silk surfaces. As shown in Figure 5a, a B-CDs concentration-dependent reduction in bacterial colonization is observed from the control to the B-CDs0.5‰ group, accompanied by the membrane collapse and the cellular rupture of *S. aureus* cells on the silk surface.[63] To quantitatively verify the membrane integrity loss, we measured the leakage of intracellular proteins (via bicinchoninic acid assay) and *β*-galactosidase (via ortho-nitrophenyl-*β*-galactoside hydrolysis) in coculture supernatants. Figure 5b,c demonstrate that both B-CDs0.1‰ and B-CDs0.5‰ groups show significantly elevated levels of cytoplasmic components ($p < 0.01$ vs. Control), confirming the disruptive effect of B-CDs@silk on the bacterial envelopes. To elucidate the changes in silk protein composition, we performed comparative proteomic analyses using three cocoons from the control and the B-CDs-treated groups, respectively. The volcano plot (Figure 5d) illustrates protein expression patterns, where gray dots represent proteins with insignificant changes (constituting the majority), while blue and red dots denote significantly downregulated and upregulated proteins, respectively.

Comprehensive protein identification is provided in Table S3. The subsequent heatmap analysis (Figure 5e) reveals distinct expression profiles of differentially expressed proteins, with blue and red coloration indicating the decreased and the increased relative expression levels, respectively, where the color intensity correlates with the magnitude of changes. Several upregulated protease inhibitors are identified, including Serpin-13, Pept_C1 domain-containing protein, and Inhibitor_I29 domain-containing protein,[64–66] which interfere with bacterial cell wall and membrane biosynthesis and suppress essential bacterial enzyme production, thereby cooperating synergistically with antibacterial activity of B-CDs.[67–70] Figure 5f illustrates such a synergistic antibacterial mechanism, in which the bacterial cell walls and cell membranes are damaged, and the enzyme inhibition effect causes the leakage of bacterial contents, thereby achieving the stronger antibacterial effect than that of sole B-CDs. To further evaluate the antimicrobial spectrum of B-CDs@silk, additional antibacterial tests were performed against the Gram-negative bacterium *Escherichia coli* (Figure S15). The B-CDs0.5‰ group reduced viable *E. coli* counts to

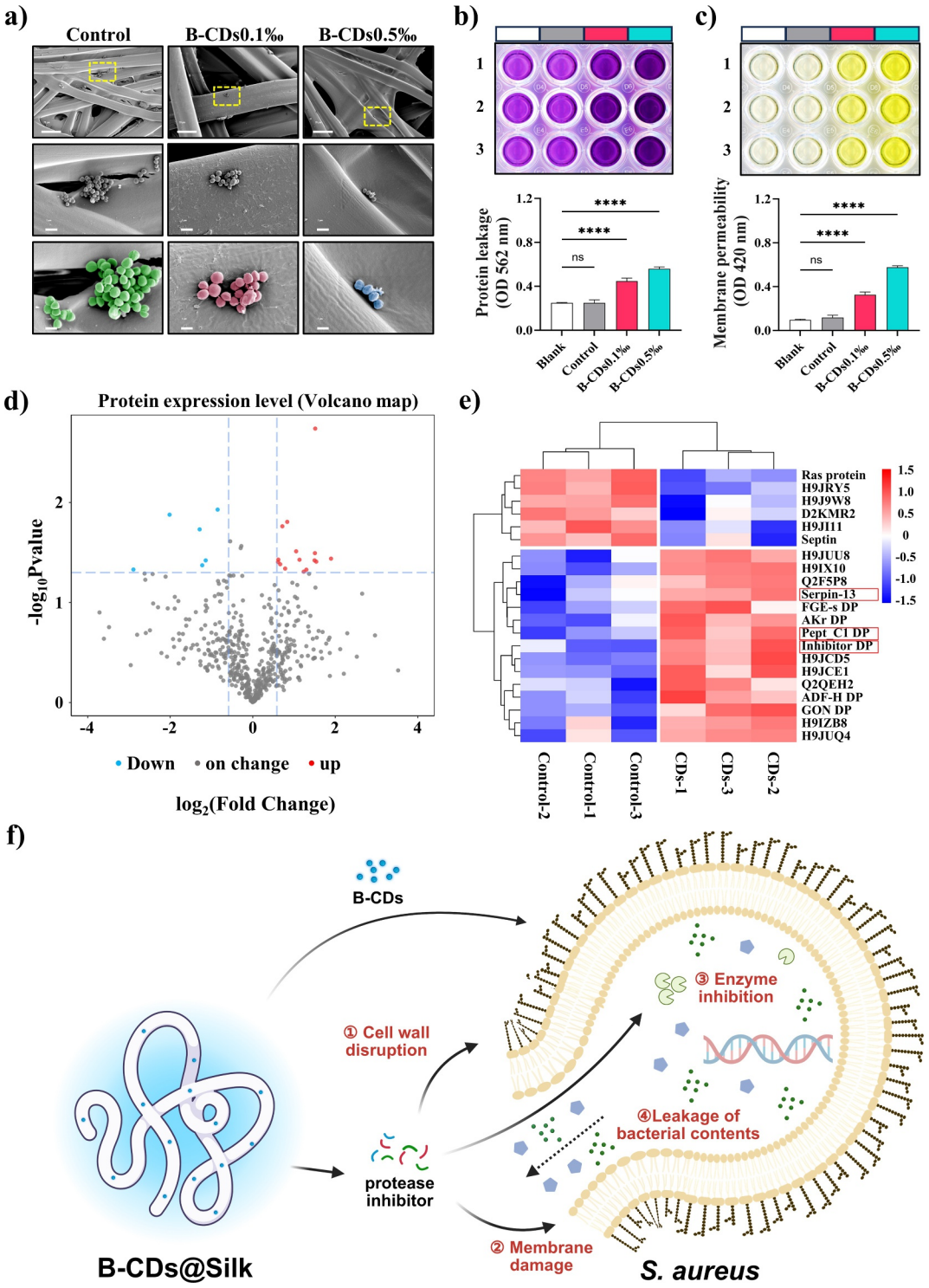

FIGURE 5 Exploration on the antibacterial mechanism of B-CDs@Silk. (a) Scanning electron microscopy images of *Staphylococcus aureus* colonization on the degummed silk surfaces. (b) Bicinchoninic acid assay for assessing the protein leakage from *S. aureus*. (c) *o*-nitrophenyl-β-D-galactopyranoside assay for evaluating the bacterial membrane permeability. (d) Volcano plot showing differential protein expression in B-CDs@silk versus that in control silk. (e) Heatmap of differentially expressed proteins in the degummed silk from the control and the experimental groups, respectively. (f) Schematic diagram for the synergistic antibacterial mechanism of the B-CDs and the upregulated antibacterial proteins in B-CDs@silk. B-CDs, blue fluorescence carbon dots.

approximately 50% of the blank control, indicating a meaningful inhibitory effect, while the B-CDs0.1‰ group showed a trend toward inhibition that did not reach statistical significance. As the two tests were conducted on silk from different feeding batches, a direct quantitative comparison with the anti-*S. aureus* results is not straightforward.

Nonetheless, given the additional LPS-containing outer membrane of Gram-negative bacteria serving as a permeability barrier,[71,72] the efficacy against *E. coli* may be inherently limited compared with that against Gram-positive bacteria.

2.6 | Metabolism and conversion rate of B-CDs in the silkworm body

B-CDs metabolism in the silkworm body was investigated by visualizing the fluorescence in silkworm tissues and recording the fluorescence evolution of the tissue extracts. Silkworms were dissected on the fourth, sixth days of the fifth instar, and at the cocooning stage, respectively. Dark-field fluorescence images of the silk glands (Figure 6a) show that the control exhibits weak autofluorescence, but as the cocooning time approaches, more and more yellow fluorescent substances (flavonoids) emerge in the silk glands.[73,74] In contrast, B-CDs0.5‰ group silk glands consistently show bright blue fluorescence, indicating progressive enrichment of B-CDs therein. Figure 6b shows the fluorescence spectra of DCM extracts from the silk glands, in which the experimental groups have a distinct blue fluorescence peak, whose intensity gradually increases with the B-CDs feeding days, until the cocooning stage. Figure 6c shows that the fluorescence spectra of the DCM extracts from silkworm feces in the experimental groups are similar to those from the silk glands.[18] TEM images of the extracts (Figure 6d,e) directly confirm the presence of B-CDs in both the silk glands and feces. The detailed bright/dark-field images (Figure S16) show more pronounced silk gland fluorescence contrast at the cocooning period, with yellow fluorescence from digested mulberry leaves and blue fluorescence in the posterior digestive tract of the experimental groups. Upon silkworm moth emergence in Figure S17, the experimental moths have blue fluorescence in their body segments, while the control moths exhibit no fluorescence at all, indicating that a fraction of B-CDs remains in silkworm bodies after weaving cocoons. Just like the previous research

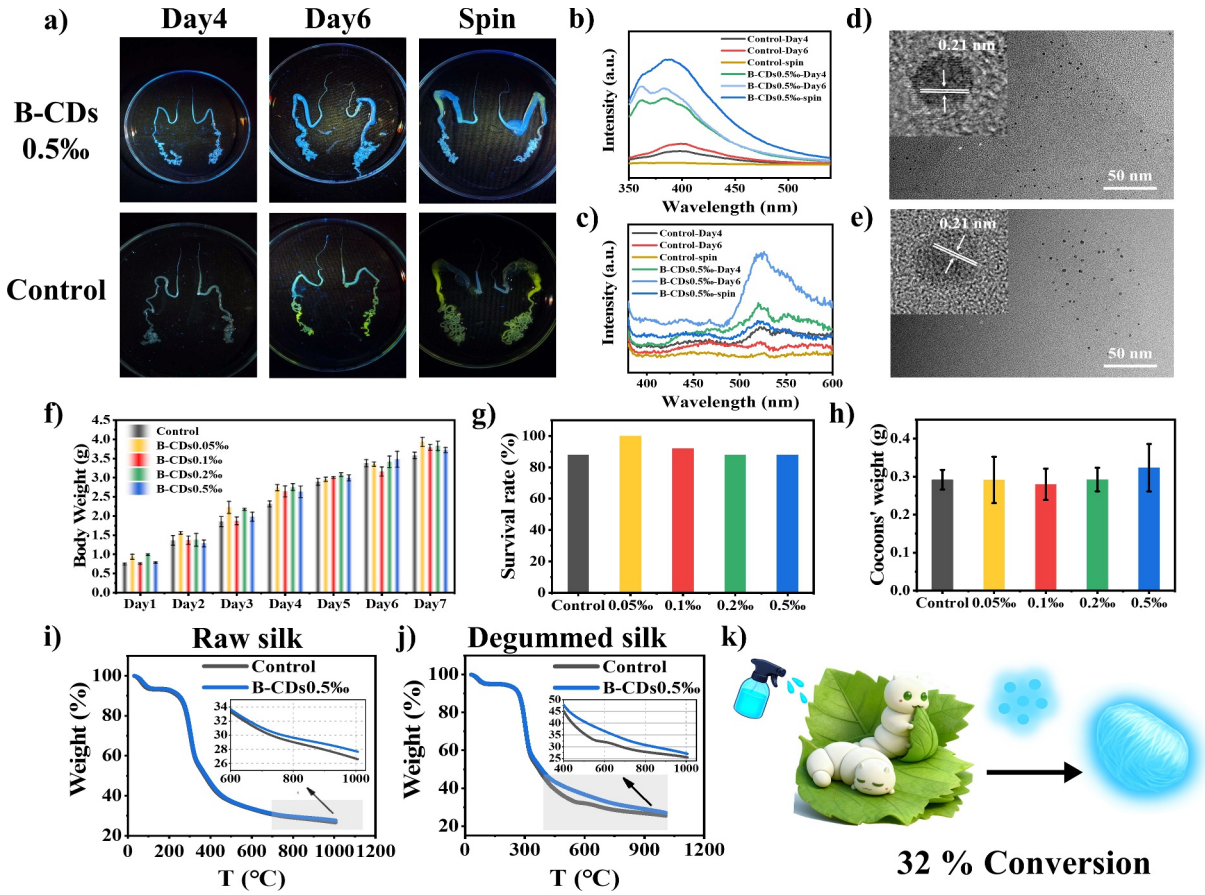

FIGURE 6 Analyses on the metabolism process and the conversion rate of B-CDs in the silkworm body. (a) Under UV light, silk glands dissected from different groups on the fourth, sixth days of the fifth instar, and during cocooning on the eighth day, respectively. (b) Fluorescence spectra of DCM extracts from the silk glands in panel (a) (ex = 330 nm). (c) Fluorescence spectra of DCM extracts from silkworm feces on the fourth, sixth days of the fifth instar, and during cocooning on the eighth day, respectively (ex = 365 nm). TEM and high-resolution TEM images of DCM extracts from (d) silk glands and (e) feces of the experimental group, respectively. (f) Body weight records of silkworms from the first day to the seventh day of the fifth instar. (g) Survival rates of silkworms in each group. (h) Weights of dry cocoons from each group after removing silkworm moths and drying at 60°C for 48 h. Thermogravimetric curves of (i) the raw silk and (j) the degummed silk, respectively. Inset: Magnified curves of the shaded areas. (k) Conversion rate of B-CDs fed to silkworms, calculated by the average intake amount and the weight of B-CDs in the silk. B-CDs, blue fluorescence carbon dots; DCM, dichloromethane; TEM, transmission electron microscopy.

employing other CDs as feed additives,[44] there are no morphological/fluorescence differences between eggs from the experimental silkworms and from the control group (Figure S18), confirming that B-CDs feeding does not induce transgenerational inheritance, and all eggs hatched normally with newborn silkworms completing their natural lifecycles.

To assess B-CDs' impact on the silkworm health, the weights of silkworms were recorded throughout the fifth instar.[75] In Figure 6f, all experimental silkworms exhibit similar weight gain to the control group with no statistical difference in maximum body weight. The survival rates across groups were comparable (Figure 6g), suggesting B-CDs are well-tolerated by silkworms. Additionally, no overt adverse effects on rat internal organs were detected (Figure S19) after wound healing. These results provide an initial indication of biosafety for both silkworms and rats. However, it should be noted that the current assessment relies on growth trends, survival rates, and histopathological observation, and more systematic toxicological evaluation covering blood biochemistry, inflammatory response markers, and organ function analysis for both animal models warrants further investigation. Figure 6h shows that experimental cocoons are not lighter than the control, and the B-CDs0.5‰ group are even heavier, suggesting the higher output of B-CDs@silk.[53] Since B-CDs exhibit a higher decomposition temperature than the cocoons, thermogravimetric (TG) analyses were performed on the cocoons and the degummed silk to assess their compositions.[76] After calcination, the final weight of the B-CDs0.5‰ cocoons is a little higher than that of the control cocoons, suggesting about 1.0 wt.% of B-CDs exist in the B-CDs0.5‰ cocoons (Figure 6i). As for the degummed silk, the TG results show about 1.5 wt.% of the residual mass corresponds to B-CDs (Figure 6j), indicating that B-CDs are enriched more in the silk fibroin and extensively retained after the degumming process.[35,77] Since the average weight of the dry cocoons from the B-CDs0.5‰ group is about 0.32 g (Figure 6h), the approximate amount of B-CDs in every dry cocoon is 3.2 mg. From the third day of the fifth instar to the cocoon-spinning stage, a single silkworm ingests approximately 20 g of mulberry leaves.[78] And thus, the conversion rate of B-CDs can be evaluated roughly through dividing the average B-CDs content in one cocoon (ca. 3.2 mg) by the average amount of B-CDs ingested per silkworm (ca. 10 mg), resulting in a conversion rate of 32% for the B-CDs0.5‰ group (Figure 6k). The above experiments demonstrate that, B-CDs are ingested by silkworms, partially excreted in feces, partially accumulated in the digestive tracts, partially retained in moths, and partially transformed into silk within the silk glands, while their last translocation is the key conversion (intake-to-silk) for B-CDs@silk.

To further evaluate whether B-CDs feeding influences the silkworm gut microbiota, full-length 16S rRNA gene amplicon sequencing was performed on fecal samples from Control and B-CDs-fed larvae ($n = 5$ per group, detailed experimental procedures are provided in the Supporting Information S1),[79] as illustrated in Figure S20a. Alpha-diversity indices (Chao1: $p = 0.7452$; Shannon: $p = 0.4506$; Figure S20b,c) showed no significant differences between groups, while PCoA revealed a significant difference in overall community composition (PERMANOVA: $R^2 = 0.288$, $P = 0.006$, Figure S20d). Phylum-level profiling suggested reduced abundance of Proteobacteria/Enterobacteriaceae-associated taxa in the B-CDs-fed group (Figure S20e), and three genera (*Kluyvera*, *Enterobacter*, and *Citrobacter*) were significantly reduced at the genus level (FDR <0.05, Figure S20f–i). Within the latter two genera, *Enterobacter* sp. and *Citrobacter freundii* have been reported to possess cellulolytic and xylanolytic activities in the silkworm gut,[80] suggesting a potential role in mulberry leaf digestion, though the genus-level reduction did not affect silkworm growth or cocoon yield (Figure 6f–h). Given that B-CDs were directly detected within the silk glands (Figure 6a, d), the upregulation of antibacterial proteins in silk is more likely attributable to the direct interaction between B-CDs and silk gland tissue/proteins than to microbiota-mediated effects. The reasons underlying these microbial changes, and whether and how they contribute to the observed silk proteomic responses, warrant further investigation.

3 | CONCLUSIONS

In summary, the main achievement of this work is producing antibacterial silk naturally by feeding silkworms with B-CDs which are derived from human hair. The new concepts and innovations of the present research lie in three aspects. Firstly, we found the traditional Chinese medicine *C. carbonisatus* contains CDs with blue fluorescence and bioactivity. Secondly, such B-CDs are nontoxic to silkworms, and they can remain in silkworm body, especially in the silk to show their stable fluorescence and antibacterial capacity. Thirdly, we found B-CDs incorporation leads to the upregulation of several antibacterial proteins in silk, thereby forming a synergistic antibacterial effect. As a result, B-CDs@silk can be used as gauze to cover wounds on rat skin, which accelerates the wound healing, promotes granulation tissue growth, and reduces scarring significantly. The hypothesis of our work is feeding silkworms with antibacterial CDs could produce natural antibacterial silk, just like those reported fluorescent silk obtained by feeding silkworms with CDs. All experimental results prove our success that the natural antibacterial silk can be obtained by feeding silkworms with the selected CDs. This achievement is much more meaningful than the fluorescent silk or the strengthened silk, because it overcomes the shortcoming of natural silk that plays hotbed for nourishing bacteria, and it is more challenging to find an antibacterial feed (nontoxic to silkworms but fatal to bacteria) that is biocompatible with both silkworms and silk. In comparison with those previously reported silk containing nano-additives, our B-CDs@silk is also outstanding in two aspects. One is the high conversion rate of 32% for B-CDs transport from intake to cocoons. The other is after degumming to remove sericin, the remained fibroin has a high content of B-CDs up to 1.5 wt.%.

Therefore, our present work confirms the feasibility of large-scale production of both fluorescent and antibacterial silk by feeding silkworms with well-selected CDs.

AUTHOR CONTRIBUTIONS

Zhao-Fan Wu and Xiao-Feng Shi performed the experiments and wrote the original draft. Xiao-Xiao Luo and Xi-Rong Zhang took part in data curation and result analysis. Yuan-Qing Mao directed the biomedical experiments. Huan-Ming Xiong supervised the whole research and revised the manuscript.

ACKNOWLEDGMENTS

This research was funded by the National Natural Science Foundation of China (22575057), the Science and Technology Commission of Shanghai Municipality (25ZR1401024), and the Shanghai Municipal Commission of Health and Family Planning (2022JC031).

CONFLICT OF INTEREST STATEMENT

The authors declare no conflicts of interest.

DATA AVAILABILITY STATEMENT

The data that support the findings of this study are available from the authors upon reasonable request.

ETHICS STATEMENT

All silkworm experiments were performed in accordance with the Guide for the Care and Use of Laboratory Animals and approved by the Department of Laboratory Animal Science at Fudan University with the approval number of 2025-CHEM-017. All rat experiments were performed in accordance with the Guidelines for Care and Use of Laboratory Animals of Shanghai Jiao Tong University School of Medicine and the national guidelines of China. The experiments were approved by the Animal Ethics Committee (Animal Research Committee) of the Ninth People's Hospital (Approval No. SH9H-2023-A91-1).

ORCID

Xiao-Feng Shi https://orcid.org/0009-0002-9855-6981
Yuan-Qing Mao https://orcid.org/0000-0002-9613-9247
Huan-Ming Xiong https://orcid.org/0000-0002-3118-942X

REFERENCES

1. Y. Wang, J. Ren, Z. Lv, L. Cao, S. Lin, Y. Pei, Q. Zhang, Z. Shao, S. Ling, *Chem. Eng. J.* **2022**, *435*, 134901.
2. H. Lu, M. Jian, X. Liang, Y. Wang, J. Niu, Y. Zhang, *Adv. Mater.* **2024**, *36*, 2408385.
3. P. Shen, S. Xu, D. Li, Y. Lin, Y. Zhang, J. Huang, X. Wang, J. Xu, W. Teng, Y. Shen, M. Liu, Z. Shen, Y. Hu, *Energy Storage Mater.* **2025**, *81*, 104464.
4. Q. Lv, S. Chen, D. Luo, H. Liu, Y. Song, M. Liu, F. Xiao, Z. Wang, L. Wang, *Adv. Mater.* **2025**, *37*, 2413610.
5. K. Yang, J. Zhang, C. Zhang, J. Guan, S. Ling, Z. Shao, *Chem. Soc. Rev.* **2025**, *54*, 4973.
6. Q. Lv, Q. Li, P. Cao, C. Wei, Y. Li, Z. Wang, L. Wang, *Adv. Mater.* **2025**, *37*, 2411946.
7. W. Fu, B. Yu, D. Ji, Z. Zhou, X. Li, R. Wang, W. Lu, Y. Sun, Y. Dai, *Responsive Mater.* **2024**, *2*, e20240018.
8. Y. Ren, B. Yan, P. Wang, Y. Yu, L. Cui, M. Zhou, Q. Wang, *ACS Sustainable Chem. Eng.* **2022**, *10*, 2192.
9. S. Kaushik, M. K. Sarma, P. D. Thungon, M. Santhosh, P. Goswami, *J. Colloid Interface Sci.* **2016**, *479*, 251.
10. S. Ghalei, H. Handa, *Mater. Today Chem.* **2022**, *23*, 100673.
11. Y. Zhou, Z.-Y. Yang, R.-C. Tang, *J. Cleaner Prod.* **2018**, *170*, 940.
12. J. Xue, H.-L. Gao, X.-Y. Wang, K.-Y. Qian, Y. Yang, T. He, C. He, Y. Lu, S.-H. Yu, *Angew. Chem. Int. Ed.* **2019**, *58*, 14152.
13. S. Guo, Y. Mu, M. Ma, W. Zhou, *Int. J. Biol. Macromol.* **2025**, *311*, 144038.
14. C. Zhou, Q. Tang, S. Yang, G. Zhao, T. Wang, Z. Chen, Y. Zhang, P. Tan, X. Ma, *Responsive Mater.* **2025**, *3*, e20240043.
15. W. Sun, M. Li, D. Nan, J. Zhao, Y. Chen, Y. Gao, S. Zhang, K. L. Van Landuyt, M. Qi, *Responsive Mater.* **2026**, e70059.
16. X.-Q. Jin, J.-L. Li, J. Liu, L.-L. Chen, C. Liu, Y.-Q. Zhou, W.-P. Shi, H. Liang, W.-H. Guo, D.-C. Yin, *Bioprocess Biosyst. Eng.* **2025**, *48*, 725.
17. H. Liu, Z. Sun, C. Guo, *Adv. Fiber Mater.* **2022**, *4*, 705.
18. J. Li, Y. Li, S. Lu, J. Zhang, C. Zhang, L. Xiong, *Adv. Fiber Mater.* **2022**, *4*, 845.
19. H. Lu, M. Jian, Z. Yin, K. Xia, S. Shi, M. Zhang, H. Wang, X. Liang, W. Ma, X. Zhang, Y. Zhang, *Adv. Fiber Mater.* **2022**, *4*, 547.
20. F. Wang, H. Lei, C. Tian, Y. Ji, F. Wang, H. Deng, H. Zhou, S. Chen, Y. Zhou, Z. Meng, M. He, S. Yang, H. Dong, D. Tu, H. Wang, X. Li, D. L. Kaplan, Q. Xia, *Adv. Mater.* **2025**, *37*, 2414878.
21. Z.-F. Wu, Z.-N. Sun, H.-M. Xiong, *Chin. J. Chem.* **2023**, *41*, 2035.
22. J. Liu, T. Kong, H.-M. Xiong, *Adv. Mater.* **2022**, *34*, 2200152.
23. S. Fan, X. Zheng, Q. Zhan, H. Zhang, H. Shao, J. Wang, C. Cao, M. Zhu, D. Wang, Y. Zhang, *Nano-Micro Lett.* **2019**, *11*, 75.
24. H. Lu, M. Jian, L. Gan, Y. Zhang, S. Li, X. Liang, H. Wang, M. Zhu, Y. Zhang, *Sci. Bull.* **2023**, *68*, 2973.
25. Q. Wang, C. Wang, M. Zhang, M. Jian, Y. Zhang, *Nano Lett.* **2016**, *16*, 6695.
26. Z.-F. Wu, B.-J. Wang, J.-W. Ni, Z.-N. Sun, X.-R. Zhang, H.-M. Xiong, *Nano Lett.* **2024**, *24*, 9675.
27. J. Liang, X. Zhang, C. Yan, Y. Wang, M. L. Norton, X. Wei, C. Donley, Y. Zhu, P. Xiao, Y. Zhang, *Mater. Des.* **2020**, *196*, 109137.
28. B. Ran, L. Ran, Z. Wang, J. Liao, D. Li, K. Chen, W. Cai, J. Hou, X. Peng, *Chem. Rev.* **2023**, *123*, 12371.
29. H. Zhang, Y. Liu, S. Qu, *Responsive Mater.* **2024**, *2*, e20240012.
30. A. T. Krasley, E. Li, J. M. Galeana, C. Bulumulla, A. G. Beyene, G. S. Demirer, *Chem. Rev.* **2024**, *124*, 3085.
31. Y. Zhang, Y. Yang, S. Ding, X. Zeng, T. Li, Y. Hu, S. Lu, *Adv. Mater.* **2025**, *37*, 2418118.
32. B. Unnikrishnan, A. Anand, C.-J. Lin, C.-Y. Lee, A. Nain, P. Srivastava, R.-S. Wu, H.-W. Chu, C.-Y. Wang, R.-H. Shi, K.-H. Lee, J.-X. Chen, J. S. Pandey, J.-Y. Lai, C.-C. Huang, H.-T. Chang, *Coord. Chem. Rev.* **2025**, *534*, 216552.
33. H. Chen, K. Luo, C. Xie, L. Zhou, *Chem. Eng. J.* **2024**, *496*, 153915.
34. Z.-F. Wu, X.-X. Luo, X.-F. Shi, B.-J. Wang, H.-W. Sun, Z.-N. Sun, Y.-Q. Mao, H.-M. Xiong, *Nanoscale* **2025**, *17*, 4958.
35. Y. Liu, L. Zhang, H. Cai, X. Qu, J. Chang, G. I. N. Waterhouse, S. Lu, *Sci. Bull.* **2024**, *69*, 3127.
36. G. A. Rajesh, V. L. John, A. P. Santhosh, A. K. N. Ambika, V. T. Puthiyedath, *Part. Part. Syst. Charact.* **2022**, *39*, 2200017.
37. V. L. John, A. R. Nayana, T. R. Keerthi, K. A. Athira Krishnan, B. C. P. Sasidharan, T. P. Vinod, *Macromol. Biosci.* **2023**, *23*, 2300081.
38. R. Tian, F. Luo, Y. Yu, J. Mi, X. Gao, Z. Wang, Y. Xie, *J. Mater. Chem. B* **2025**, *13*, 6855.
39. Y. Zhang, S. Wang, F. Lu, M. Zhang, H. Kong, J. Cheng, J. Luo, Y. Zhao, H. Qu, *J. Nanobiotechnol.* **2021**, *19*, 257.
40. X. Shi, Q. Ma, X. Jia, Z. Wu, C. Yu, T. Gao, W. Xu, Z. Sun, J. Zhang, H. Xiong, Y. Mao, *Small Struct.* **2025**, *6*, 2400435.
41. T.-B. Song, Q.-L. Ma, B.-J. Wang, X.-R. Zhang, Y.-G. Wang, H.-M. Xiong, *Angew. Chem. Int. Ed.* **2025**, *64*, e202503655.
42. X. Huang, X. Jin, H. Bai, B. Huang, X. Zhang, J. Zuo, X. Ma, L. Ding, H. Zhou, X. Feng, W. Chen, *Adv. Mater.* **2025**, *37*, 2418335.

43. Y. Ma, X. Chen, H. Javeria, Z. Du, *J. Chromatogr. B* **2023**, *1227*, 123804.
44. N. C. Tansil, Y. Li, L. D. Koh, T. C. Peng, K. Y. Win, X. Y. Liu, M.-Y. Han, *Biomaterials* **2011**, *32*, 9576.
45. X.-R. Zhang, T.-B. Song, T.-L. He, Q.-L. Ma, Z.-F. Wu, Y.-G. Wang, H.-M. Xiong, *Adv. Funct. Mater.* **2025**, *35*, 2419219.
46. K. Jiang, J. Jiang, Z. Cheng, H. Cui, J. Zhang, H. Lin, *Responsive Mater.* **2026**, e70057. https://doi.org/10.1002/rpm2.70057
47. W.-J. Zheng, Z.-N. Sun, Y.-M. Wang, H.-M. Xiong, *Nano Res.* **2024**, *17*, 8495.
48. L. Jiang, H. Cai, W. Zhou, Z. Li, L. Zhang, H. Bi, *Adv. Mater.* **2023**, *35*, 2210776.
49. J.-W. Ni, X.-R. Zhang, T.-B. Song, Z.-H. Huang, Q.-L. Ma, T.-L. He, H.-M. Xiong, *Chem. Eng. J.* **2024**, *500*, 157379.
50. X.-R. Zhang, H.-W. Sun, L. Xiao, Z.-F. Wu, H.-M. Xiong, *Responsive Mater.* **2026**, e70050. https://doi.org/10.1002/rpm2.70050
51. Z. Hu, Y. Liang, S. Fan, Q. Niu, J. Geng, Q. Huang, B. S. Hsiao, H. Chen, X. Yao, Y. Zhang, *Adv. Mater.* **2024**, *36*, 2410007.
52. J. Du, Z. Yang, H. Lin, D. Poelman, *Responsive Mater.* **2024**, *2*, e20240004.
53. Q. Zhan, S. Fan, D. Wang, X. Yao, H. Shao, Y. Zhang, *Compos. Commun.* **2020**, *21*, 100414.
54. Y. Zhang, M. Zhang, W. Li, T. Hu, Y. Liu, H. Huang, Z. Kang, *Int. J. Biol. Macromol.* **2024**, *281*, 136644.
55. M. Wang, Z. Du, A. Tong, Y. Zhang, Y. Luo, Z. Shi, S. Qiao, Z. Huang, A. He, X. Chen, G. Ke, Q. Liu, W. Xu, F. Chen, *Small Struct.* **2025**, *6*, 2400639.
56. Z.-P. Zhang, M. Khurshid, S.-H. Li, Y.-J.-C. Li, L. Quaye, R. A. Herman, J. Wang, *ACS Appl. Nano Mater.* **2025**, *8*, 3129.
57. M. Mizushima, T. Mizuno, M. Toda, M. P. Williamson, Y. Suzuki, *J. Am. Chem. Soc.* **2025**, *147*, 36805.
58. D. Gao, X. Yang, B. Lyu, L. Xue, Y. Wei, J. Ma, S. Zhou, *J. Colloid Interface Sci.* **2025**, *680*, 689.
59. Z. Lu, M. Meng, Y. Jiang, J. Xie, *Colloids Surf., A* **2014**, *447*, 1.
60. B. Guo, Y. Liu, S. Han, P. Wu, W. Xu, X. Ma, Z. Zhang, S. Peng, J. Hu, S. Chen, L. Yang, *Eur. Polym. J.* **2024**, *215*, 113230.
61. X. Meng, Y. Tang, Q. Li, *Responsive Mater.* **2025**, *3*, e20250021.
62. A. Bassam, M. Du, Y. Li, X. He, *Responsive Mater.* **2025**, *3*, e20240031.
63. S. Qiao, Z. Shi, A. Tong, Y. Luo, Y. Zhang, M. Wang, Z. Huang, W. Xu, F. Chen, *Adv. Colloid Interface Sci.* **2025**, *341*, 103500.
64. Y. He, Y. Wang, P. Zhao, S. Rayaprolu, X. Wang, X. Cao, H. Jiang, *Insect Biochem. Mol. Biol.* **2017**, *90*, 71.
65. J.-S. Zhang, J. Li, J.-Y. Meng, X. Tang, H. Saddique, C.-Y. Zhang, *Sci. Rep.* **2025**, *15*, 25214.
66. Y.-X. Sun, C. Chen, W.-J. Xu, M. N. Abbas, F.-F. Mu, W.-J. Ding, H.-J. Zhang, J. Li, *Dev. Comp. Immunol.* **2021**, *116*, 103927.
67. Y. Li, P. Zhao, S. Liu, Z. Dong, J. Chen, Z. Xiang, Q. Xia, *Insect Biochem. Mol. Biol.* **2012**, *42*, 766.
68. Z. Dong, Q. Xia, P. Zhao, *Int. J. Biol. Macromol.* **2023**, *224*, 68.
69. Y.-S. Li, H.-W. Liu, R. Zhu, Q.-Y. Xia, P. Zhao, *Insect Sci.* **2016**, *23*, 835.
70. L. Wang, L. Shi, B. Xu, L. Zhou, T. Chen, C. Yang, M. Jin, Y. Wang, *Responsive Mater.* **2026**, *4*, e70040.
71. B. W. Simpson, M. S. Trent, *Nat. Rev. Microbiol.* **2019**, *17*, 403.
72. C. Zhou, Q. Tang, P. Tan, T. Wang, Y. Zhang, S. Yang, G. Zhao, Y. Feng, X. Ma, *Responsive Mater.* **2025**, *3*, e20240029.
73. C. Hirayama, H. Ono, Y. Meng, T. Shimada, T. Daimon, *Phytochemistry* **2013**, *94*, 108.
74. S. Napavichayanun, O. Lutz, M. Fischnaller, T. Jakschitz, G. Bonn, P. Aramwit, *Arch. Biochem. Biophys.* **2017**, *631*, 58.
75. X. Zheng, M. Zhao, H. Zhang, S. Fan, H. Shao, X. Hu, Y. Zhang, *ACS Biomater. Sci. Eng.* **2018**, *4*, 4021.
76. Y. Liu, L. Yang, C. Ma, *J. Therm. Anal. Calorim.* **2020**, *139*, 589.
77. N. C. Tansil, Y. Li, C. P. Teng, S. Zhang, K. Y. Win, X. Chen, X. Y. Liu, M.-Y. Han, *Adv. Mater.* **2011**, *23*, 1463.
78. R. Alisher, S. Sharifjon, R. Akmal, *Engineering* **2019**, *11*, 755.
79. F. Lu, D. Guan, X. Zhang, J. Wei, J. Song, F. Qian, *Appl. Soil Ecol.* **2025**, *207*, 105952.
80. A. A. P. Anand, S. J. Vennison, S. G. Sankar, D. I. G. Prabhu, P. T. Vasan, T. Raghuraman, C. J. Geoffrey, S. E. Vendan, *J. Insect Sci.* **2010**, *10*, 1.

SUPPORTING INFORMATION

Additional supporting information can be found online in the Supporting Information section at the end of this article.

How to cite this article: Z.-F. Wu, X.-F. Shi, X.-X. Luo, X.-R. Zhang, Y.-Q. Mao, H.-M. Xiong, *Responsive Mater*. **2026**, e70074. https://doi.org/10.1002/rpm2.70074